Highly Decoupled Graphene Multilayers: Turbostraticity at its Best

ARTICLE *in* JOURNAL OF PHYSICAL CHEMISTRY LETTERS · OCTOBER 2015

Impact Factor: 7.46 · DOI: 10.1021/acs.jpclett.5b02145

THE JOURNAL OF PHYSICAL CHEMISTRY Letters

Letter

pubs.acs.org/JPCL

Highly Decoupled Graphene Multilayers: Turbostraticity at its Best

Umesha Mogera,[†] Radhakrishnan Dhanya,[†] Rajashekhar Pujar,[†] Chandrabhas Narayana,[†] and Giridhar U. Kulkarni*[,‡,§]

[†]Chemistry and Physics of Materials Unit and Thematic Unit on Nanochemistry, Jawaharlal Nehru Centre for Advanced Scientific Research, Jakkur P.O., Bangalore 560064, India

[‡]Centre for Nano and Soft Matter Sciences, Jalahalli P.O., Bangalore, 560013, India

Supporting Information

ABSTRACT: The extraordinary properties of graphene are truly observable when it is suspended, being free from any substrate influence. Here, a new type of multilayer graphene is reported wherein each layer is turbostratically decoupled, resembling suspended graphene in nature, while maintaining high degree of 2D crystallinity. Such defect-free graphene multilayers have been made over large areas by Joule heating of a Ni foil coated with a solid hydrocarbon. Raman spectra measured on thick flakes of turbostratically single layer graphene (T-SLG) (100−250 nm) have shown characteristics similar to suspended graphene with very narrow 2D bands (∼16 cm^{-1}) and I_{2D}/I_G ratios up to 7.4, importantly with no D band intensity. Electron diffraction patterns showed sets of diffraction spots spread out with definite angular spacings, reminiscent of the angular deviations from the AB packing which are responsible for keeping the layers decoupled. The *d*-spacing derived from X-ray diffraction was larger (by ∼0.04 Å) compared to that in graphite. Accordingly, the *c*-axis resistance values were three orders higher, suggesting that the layers are indeed electronically decoupled. The high 2D crystallinity observed along with the decoupled nature should accredit the observed graphene species as a close cousin of suspended graphene.

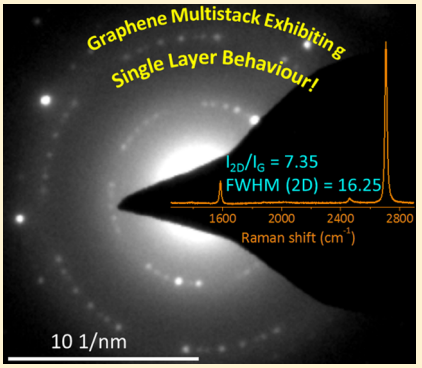

Graphene as a two-dimensional carbon material offers wide range of interesting properties such as high charge mobilities,[1] superior thermal conductivity,[2] high degree of transparency,[3] as well as mechanical flexibility[4] among others. Because of such properties, it has attracted great attention in the context of flexible electronics,[5] printable optoelectronics,[6] photonics,[7] etc. Ideally, graphene has to be perfectly two-dimensional well extended and flat, for it to possess the characteristic electronic band structure and properties associated with it.[8] In reality, the properties of graphene get modified due to the presence of wrinkles,[9] edges,[10] defects[11] and also due to adsorbed foreign species[12] and dopants.[13] In addition, the substrate hosting the graphene can itself significantly influence its electronic,[14] magnetic,[15] and chemical properties[16] and such modifications, intentional and otherwise, have been effectively utilized in various contexts.[17] However, if one is serious in exploiting the native properties of graphene, it has to be prepared and handled in such a way that the above influences are minimal. One such case is the suspended graphene, which comes close to ideal graphene in nature, and therefore has attracted greater attention in recent years due to its extraordinary properties,[18] especially in order to achieve near ideal ballistic transport[19] and ultrahigh mobility in field effect transistors.[20] However, synthesis and fabrication of large-area suspended graphene reproducibly is a daunting task[21] involving several lithographic processes. The purity of the graphene produced is also under question as such steps leave behind residues from photoresists. In this context, we considered it interesting to explore turbostratic graphite as a form of suspended graphene.

Unlike normal graphite where the layers are perfectly AB stacked,[22] in turbostratic graphite there is no definite stacking order between adjacent layers. The popular form of normal graphite is the highly oriented pyrolitic graphite (HOPG), which is synthetically prepared at elevated temperatures to achieve a high degree of crystallinity.[23] In turbostratic graphite, each stacked layer is randomly rotated with respect to its adjacent layers[24] and this angular disorder causes decoupling of the adjacent layers, resulting in increased interlayer spacing (3.35 to 3.42 Å).[25] Due to the absence of the interlayer interaction, the Raman spectrum of turbostratic graphite shows signatures of single-layer graphene (SLG), namely, single Lorenztian 2D peak, but the full width at half-maximum (fwhm) (2D) is almost double that of SLG.[26] Unfortunately, Raman spectra of turbostratic graphite reported in the literature invariably contain noticeable D peak intensity implying the non-negligible presence of defects.[26] These defects are present in turbostratic graphite in the form of stacking faults and a large number of sp^3 carbon atoms.[27] Despite being a decoupled system, turbostratic graphite is considered ill-defined and not so useful solely due to its defects.

Received: September 26, 2015
Accepted: October 23, 2015

DOI: 10.1021/acs.jpclett.5b02145
J. Phys. Chem. Lett. 2015, 6, 4437−4443

Scheme 1. Classification of Different Types of Graphitic Materials Known in the Literature[a]

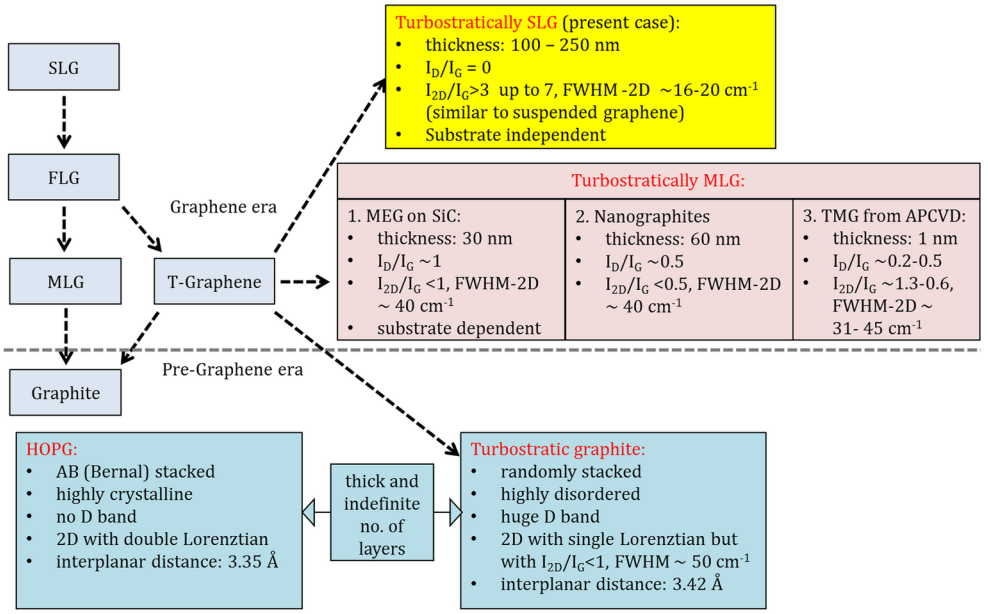

[a]Dotted bar separates the graphene related materials from graphite. SLG: single-layer graphene; FLG: few-layer graphene; MLG: multilayer graphene; T-graphene: turbostratic graphene; MEG: multilayer epitaxial graphene; SiC: Silicon carbide; T-MLG or TMG: turbostratically multilayer graphene.

Recently since the graphene era, the turbostratic nature of graphite is being revisited. Ab initio calculations using DFT have shown that few layered graphitic systems with angular stacking disorder can possess massless Fermion behavior showing Dirac cones in the electronic structure, typical of SLG.[28] Experimentally, Kim et al. studied Raman spectra of double layer graphene with varied rotation between them and found that intensity and fwhm of 2D peak varied sensitively with rotation angles.[29] Among multilayer systems, SLG-like behavior has been observed only in the case of epitaxially grown graphene (MEG) on C-terminated SiC.[30] Hass et al. have provided evidence based on low energy electron diffraction (LEED), scanning tunnelling microscope (STM) and surface X-ray diffraction (SXRD) that the adjacent graphene layers in MEG are electronically isolated from each other[31] due to angular disorder. Its Raman spectrum contained a single Lorenztian 2D peak with fwhm of 40 cm^{-1}.[32] Using glazing incidence XRD (GIXRD), it was shown that MEG consisted of both Bernal and turbostratic stackings.[33] Orlita et al. reported a mobility of 250 $kcm^2/(V\ s)$ in MEG calculated using far-infrared (FIR) transmission experiments.[34] In the above examples unfortunately, significant intensity is seen with the D band. Further, it has been reported that MEG grown on SiC loses its SLG-like behavior upon transferring onto other substrates.[35]

In this Letter, we report a new species of graphene multilayers prepared by Joule heating a hydrocarbon coated Ni foil.[36] Detailed characterization using Raman spectroscopy, conducting atomic force microscopy (C-AFM), transmission electron microscopy (TEM), and X-ray diffraction (XRD) have been carried out. The aspect which made the study worthwhile is the Raman spectrum consisting of 300−700 graphene layers showing single Lorenztian 2D peak with fwhm of 16−20 cm^{-1} with no D peak in it, resembling suspended graphene characteristics. This multilayer system may be termed as turbostratically single layer graphene (T-SLG), as detailed in Scheme 1.

The synthesis procedure is similar to our previous work[36] with minor but important modifications (see Figure 1a). Briefly,

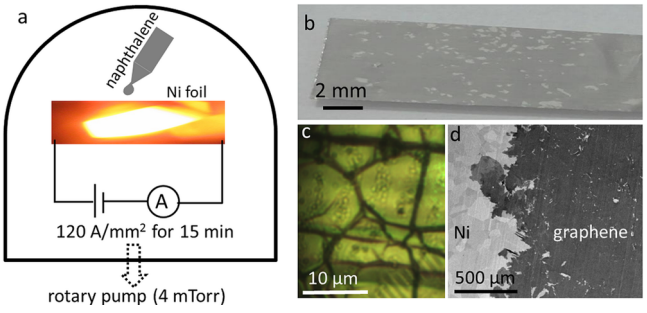

Figure 1. Synthesis and microscopy of graphene. (a) Schematic of graphene synthesis procedure. It involves drop coating of naphthalene solution on a Ni foil followed by Joule heated to red hot and cooling. (b) digital photograph, (c) optical microscopy, and (d) low magnification FESEM image of graphene on Ni. Relatively darker region in (b) is due to graphene formation on Ni.

a polycrystalline Ni foil (7 μm, 99.9%, Advent Research Materials) was taken and cut into a 4 × 0.6 cm^2 strip and connected to the current-carrying electrodes. Naphthalene solution (10 μL, 1 mM) in chloroform was drop cast onto the Ni foil and allowed to dry. After reaching a rotary vacuum of ~5 mTorr, the Ni foil was Joule heated to red hot (~800 °C) with a current density of 120−150 A/mm^2 using a DC source for 15 min and then immediately cooled. We found that the DC source produced higher yield of the desired species (Figure S1, Supporting Information). Graphene on Ni foil is visibly seen as shown in the photograph in Figure 1b. The optical microscopy image in Figure 1c shows large graphene domains surrounded by graphene wrinkles. Low magnification FESEM image in

DOI: 10.1021/acs.jpclett.5b02145
J. Phys. Chem. Lett. 2015, 6, 4437−4443

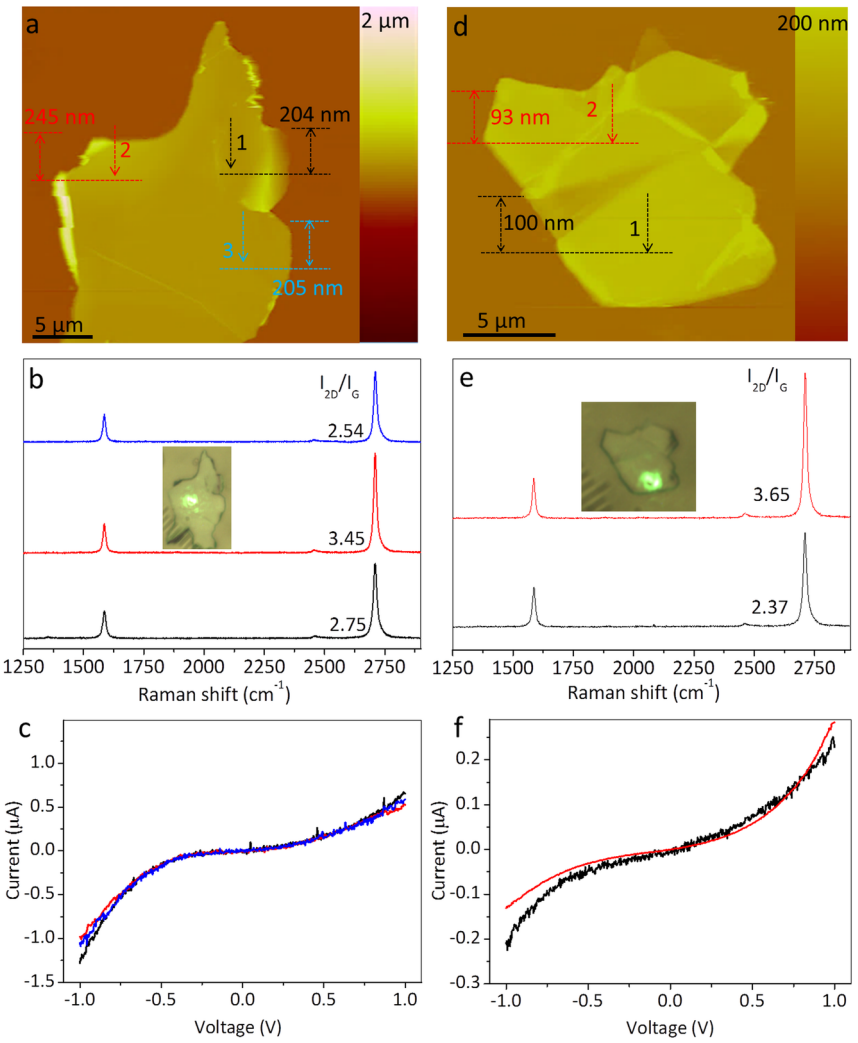

Figure 2. Raman and C-AFM measurements on T-SLG. (a,d) AFM topology of typical T-SLG flakes. Arrows marked 1 (black), 2 (red), and 3 (blue) indicate the spots where Raman and I−V measurements have been made. The flake thicknesses are shown adjacent to the spots. (b,e) Raman spectra from the corresponding regions with its I_{2D}/I_G values. Insets show optical micrographs of the T-SLG flakes with incident Raman beam. (c,f) I−V characteristics of graphene multilayers measured using conducting AFM at the designated spots.

Figure 1d, where darker regions correspond to graphene, shows uniform large area growth on Ni. The Ni polycrystalline domains are also seen.

The graphene obtained on Ni foil was transferred on to gold coated glass substrates by peeling off graphene multilayers using scotch tape. Two such multilayer flakes (flake 1 and flake 2), shown in Figure 2, are random in shape with lateral size larger than 200 μm^2. On flake 1, at different regions 1 (black), 2 (red), and 3 (blue) the thickness, as measured using AFM, was found to be approximately 204, 245, and 205 nm respectively (Figure 2a). Considering typical interplanar distance of graphite of ∼0.34 nm, the total number of layers may be counted as ∼597 ± 10, 717 ± 10 and 600 ± 10 respectively. The variations in the thickness within a flake arise due to the steps as evident from AFM images (Figure S2, Supporting Information). Raman spectra recorded on these regions (Figure 2b, optical microscopy image in the inset), surprisingly, exhibit single Lorentzian symmetric 2D band at ∼2710 cm^{-1} with the fwhm varying between 18−20 cm^{-1}, resembling SLG characteristics. The calculated I_{2D}/I_G ratios were found to be 2.75, 3.45, and 2.54, respectively, which are typical values observed for SLG (Table S1, Supporting Information, for Raman analysis). AFM topology images show that the surfaces are indeed smooth (Figure S2, Supporting Information) with local roughness of the regions being ∼1.10, 0.607, and 0.774 nm, respectively. These details clearly indicate that the obtained Raman spectra were intrinsically due to the turbostratic nature of graphene layers.

To further confirm the turbostratic nature of graphene, its *c*-axis resistance was measured using C-AFM by acquiring *I*−*V* curves on the same three regions. All the *I*−*V* curves were found to be nonlinear due to nonohmic contact between the tip and the sample (see Figure 2c). The *c*-axis resistance values calculated at −1 V were found to be 1.59, 1.81, and 1.71 MΩ respectively. These values are similar to that reported for graphene sheet measured using C-AFM.[37] As a control, the *I*−*V* characteristic of HOPG was acquired in a similar way, and its *c*-axis resistance value was measured to be merely 1.37 kΩ (Figure S3, Supporting Information), which agrees with the literature value.[38] Clearly, there is three orders increase in the *c*-axis resistance values of flake 1 compared to HOPG. The increase in resistance is solely due to the high degree of interlayer decoupling between graphene layers present in the flake.

DOI: 10.1021/acs.jpclett.5b02145
J. Phys. Chem. Lett. 2015, 6, 4437−4443

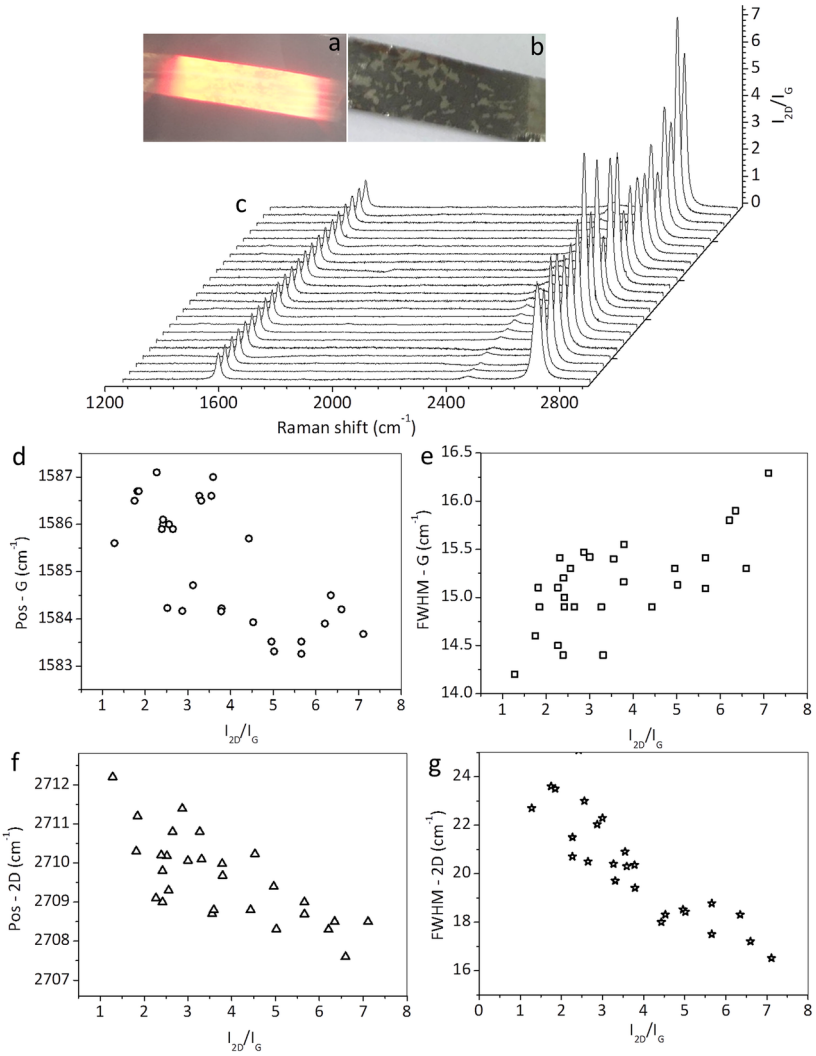

Figure 3. Raman analysis of T-SLG. (a) A photograph of Joule heating of Ni foil using DC current source. The uniform heating of foil can be seen. (b) A photograph of graphene formed on Ni foil on which Raman spectra were recorded at 22 different random regions. (c) All the spectra were normalized to G band and hence intensity of 2D band is same as I_{2D}/I_G ratios. Variations of positions of (d) G and (f) 2D and fwhm of (e) G and (g) 2D with I_{2D}/I_G ratios for T-SLG obtained from different samples.

Similarly, flake 2 was studied in detail by measuring its thickness, I_{2D}/I_G ratio and *c*-axis resistance values. At two regions 1 (black) and 2 (red), thickness was found to be 100 and 93 nm, respectively (Figure 2d) corresponding to 294 ± 10 and 273 ± 10 layers, respectively. The local surface roughness values of these two regions were calculated to be 1.17 and 1.42 nm, respectively. The Raman spectra (see Figure 2e) from these regions are very similar to those from flake 1 with I_{2D}/I_G ratios of 2.37 and 3.65 respectively. Similarly, *c*-axis resistance values were found to be 6.0 and 6.9 MΩ respectively (Table S1, Supporting Information, for Raman analysis and *c*-axis resistance values).

In the above cases, in spite of being thick, the flakes behave as SLG in Raman measurements due to decreased interlayer interaction between graphene layers. We denote these flakes as T-SLG. The striking feature of these T-SLG flakes is that the Raman spectra contain are devoid of any D peak in contrast to conventional turbostratic graphite as well as recently reported turbostratic graphene, which contain noticeable D peak intensity.[26] It is well-known that the presence of structural defects can strongly influence electronic properties of graphene,[39] the current focus on graphene research being defect-free graphene structures. Graphene obtained by other thermal methods is made defect-free by Joule heating post synthesis, aiding lattice reconstruction and self-repair of defects.[40] Since in our study, graphene synthesis itself involves Joule heating, the defects are naturally absent.

As controls, we examined conventional graphitic flakes (obtained by slightly varying synthetic conditions; see Figure S1, Supporting Information) of similar thicknesses where Raman spectra contained broad and asymmetric 2D band with I_{2D}/I_G ratio of ∼0.31, typical of Bernal graphite[41] (see details in Figure S4, Supporting Information). The *c*-axis resistances values were found to be ∼7.80 kΩ, which are nearly same as that of HOPG but three orders lower than T-SLG (*c*-axis resistance ∼1 MΩ) (Table S1, Supporting Information). For overall comparison, *I*−*V* characteristics of all flakes along with that of HOPG are presented in Figure S5a (Supporting Information). All the *c*-axis resistance values are plotted in a histogram plot (Figure S5b, Supporting Information). It is evident that flake 1 and flake 2, even though consist of more than 300 layers, tend to exhibit SLG-like Raman signatures with the I_{2D}/I_G ratios in the range 2.5−4.0. The position of 2D band is observed at 2710 cm^{-1}. The 2D bands are sharp with

DOI: 10.1021/acs.jpclett.5b02145
J. Phys. Chem. Lett. 2015, 6, 4437−4443

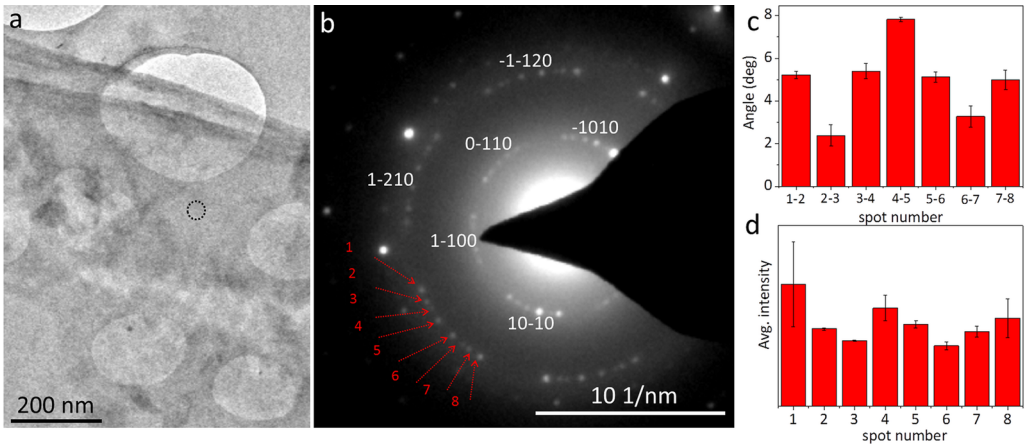

Figure 4. TEM analysis of T-SLG. (a) A bright-field TEM image of thin T-SLG flakes. (b) SAED pattern of T-SLG acquired on the dotted circle region in (a). (c,d) Histogram of angle between diffraction spots and its intensity profile of spots numbered 1 to 8 pointed by arrow mark in (a). A thin region of thickness ~15 nm was chosen, which is transparent enough for an electron beam.

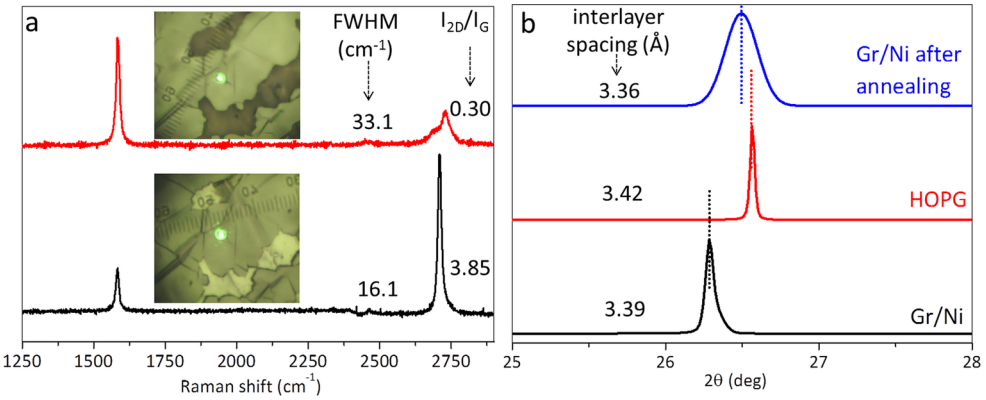

Figure 5. Effect of heating on the turbostratic nature of graphene. (a) Raman spectra recorded at the same region before (black curve) and after (red curve) heating T-SLG at ~1500 °C. Insets are optical micrographs of the same T-SLG flake with incident Raman beam. (b) X-ray diffraction pattern of T-SLG (red curve) measured in bulk compared to that of HOPG (black curve). Blue curve is the XRD of T-SLG after it is subjected to heating at ~1100 °C for an hour at ~10^{-5} Torr.

FWHMs of 18−20 cm^{-1} indicating that the graphene obtained (T-SLG) is quite different compared to conventionally obtained SLG (Table S2, Supporting Information) and other forms of turbostratic graphite/graphene known so far (see Scheme 1).

Raman spectra were recorded for many such T-SLG samples to carefully analyze the positions and widths of G and 2D bands. Raman spectra obtained from one such sample (shown in Figure 3a and 3b) is shown in Figure 3c, where the sampling area was 1 cm × 2 cm. All spectra are typical of SLG with single Lorentzian 2D band. Clearly, it can be seen that the I_{2D}/I_G ratio is greater than 3 in most locations, the maximum value being 7.4. For graphene in general, an I_{2D}/I_G ratio greater than 2 refers to SLG, a value between 1 and 2 refers to bilayer graphene (BLG), and if it is less than 1, it amounts to few-layer graphene (FLG). It is noteworthy that for chemical vapor deposition (CVD)-grown SLG lying on any substrate, it is hard to find a region with $I_{2D}/I_G > 4$.[42] Only suspended graphene routinely shows I_{2D}/I_G values more than 4,[43] rarely up to 9,[44] in the absence of any substrate influence. It is therefore not surprising that the extraordinary transport properties of graphene have been observed only in the case of suspended graphene.[18−20] We have observed I_{2D}/I_G values between 3 and 7.4 indicating that T-SLG from this study virtually behaves as suspended defect-free graphene. Similarly, other spectral features fall in line. The position and fwhm of the G band are scattered in a narrow range with increasing I_{2D}/I_G ratio, ~1587 to 1583 cm^{-1} and 14.2 to 16 cm^{-1}, respectively (Figure 3d,e). Similarly for the 2D band, the position decreases from 2712 to 2707 cm^{-1} and fwhm, from 24 to 16 cm^{-1} as I_{2D}/I_G varies between 1 and 7.4 (Figure 3f,g). This variation with I_{2D}/I_G is similar to that of suspended graphene[43] with the position of the 2D band the same (~2710 cm^{-1}) as that of turbostratic graphite.[26] Indeed, fwhm is lower than the value observed for suspended SLG (24 cm^{-1}),[43] and much lower compared to turbostratic graphite values, ~50 cm^{-1}.[45] These values are also superior when compared to CVD-grown SLG where the fwhm of 2D is ~30 cm^{-1}.[46] What is noteworthy is that, in the case of T-SLG, the fwhm and I_{2D}/I_G are insensitive to the presence of the substrate, as one would expect for thick flakes.

Angular disorder in turbostratic graphite/graphene has been a subject of investigation. In the case of MEG grown on SiC, angular mismatch values of 30° have been probed successfully using LEED and STM techniques.[31] Here we used selected area electron diffraction (SAED) technique to investigate the angular relations among T-SLG layers (Figure 4). Unlike SLG, which shows hexagonal diffraction spots,[47] and bilayer graphene which normally exhibits split spots,[48] in the present

DOI: 10.1021/acs.jpclett.5b02145
J. Phys. Chem. Lett. 2015, 6, 4437−4443

case surprisingly, each diffraction feature has split into sets of eight distinct spots (see Figure 4b). The sharpness of the spots clearly indicates the 2D crystallinity associated with the graphene layers. The angle between the split spots varies typically from 2° to 6° (see Figure 4c) which directly relates to the angular orientation between each graphene layers.[49] These correspond to superlattice reflections with varying weights depending on the number of participating layers with similar angular relation, which in turn decides the spot intensity (Figure 4d). The SAED of graphitic flakes was also acquired, which shows that typical of multilayer graphene[50] (Figure S6, Supporting Information).

Conventional turbostratic graphite is usually defect annealed at high temperature to convert to crystalline graphite.[51] We used the annealing approach to cross-examine the inherent turbostraticity in T-SLG. A T-SLG flake with I_{2D}/I_G ratio of 3.2 (Figure 5a, black curve) was placed in a molybdenum boat and was heated to ∼1500 °C for an hour at 10^{-5} Torr. Interestingly, the flake got converted to graphite with 2D band appearing at ∼2725 cm^{-1} and a left shoulder at ∼2680 cm^{-1} (Figure 5a, red curve). Accordingly, the XRD peak at 26.28° (see Figure 5b, black curve) shifted to 26.49° (blue curve) with the corresponding change in the *d*-spacing (from 3.39 to 3.36 Å). It may be noted that HOPG (red curve) exhibits the XRD peak at 26.56° (*d*-spacing is 3.35 Å). From above observations, it is clear that recrystallization (reorganization) of T-SLG has led to the graphitic form.

EXPERIMENTAL METHODS

The Raman spectra were recorded in the backscattering geometry using a 532 nm excitation from a diode pumped, frequency-doubled, Nd:YAG solid-state laser (model GDLM-5015L, Photop Suwtech, China) and a custom-built Raman spectrometer equipped with a SPEX TRIAX 550 monochromator and a liquid nitrogen cooled CCD detector (Spectrum One with CCD3000 controller, ISA Jobin Yvon).[52] After every acquisition, an optical micrograph was captured with the laser excitation Raman beam incident on the sample using Moticam-2500 camera. The morphology of the grown graphene on Ni was examined using a field emission SEM (Nova Nano SEM 600, FEI Company). AFM imaging and *I*−*V* measurement was done using a diInnova SPM (Veeco, USA) using Si_3N_4 probes (spring constant 0.1 N/m) in contact mode at a scanning force of 5 nN. Transmission electron microscopy (TEM) and selected area electron diffraction (SAED) were performed using a Technai F30 UHR nstrument operating at 200 kV. Graphene on Ni was transferred onto the holey carbon film of the Cu TEM grid by an electrochemical delamination method followed by lifting off poly(methyl methacrylate) (PMMA) using acetone. XRD was carried using a Bruker D8 Discover diffractometer, Cu Kα (1.5419 Å).

ASSOCIATED CONTENT

Supporting Information

The Supporting Information is available free of charge on the ACS Publications website at DOI: 10.1021/acs.jpclett.5b02145.

Detailed AFM analysis of T-SLG, Raman and *I*−*V* of HOPG, overall comparison of T-SLG and graphitic flakes along with HOPG, table of Raman parameters and *c*-axis resistance values of all flakes, and Raman, C-AFM measurements, and the details of graphitic flakes (PDF)

AUTHOR INFORMATION

Corresponding Author

*E-mail: kulkarni@jncasr.ac.in or gukulk@gmail.com.

Present Address

[§](G.U.K.) On lien from Jawaharlal Nehru Centre for Advanced Scientific Research, Jakkur P.O., Bangalore 560064, India.

Notes

The authors declare no competing financial interest.

ACKNOWLEDGMENTS

The authors thank Prof. C.N.R. Rao for his constant encouragement. This research work is supported by Department of Science and Technology (DST), New Delhi, India. U.M. thanks CSIR, India, and D.R. thanks UGC, India, for the research fellowship.

REFERENCES

(1) Novoselov, K. S.; Geim, A. K.; Morozov, S. V.; Jiang, D.; Zhang, Y.; Dubonos, S. V.; Grigorieva, I. V.; Firsov, A. A. Electric Field Effect in Atomically Thin Carbon Films. *Science* **2004**, *306*, 666−669.

(2) Balandin, A. A.; Ghosh, S.; Bao, W.; Calizo, I.; Teweldebrhan, D.; Miao, F.; Lau, C. N. Superior Thermal Conductivity of Single-Layer Graphene. *Nano Lett.* **2008**, *8*, 902−907.

(3) Nair, R. R.; Blake, P.; Grigorenko, A. N.; Novoselov, K. S.; Booth, T. J.; Stauber, T.; Peres, N. M. R.; Geim, A. K. Fine Structure Constant Defines Visual Transparency of Graphene. *Science* **2008**, *320*, 1308.

(4) Gomez De Arco, L.; Zhang, Y.; Schlenker, C. W.; Ryu, K.; Thompson, M. E.; Zhou, C. Continuous, Highly Flexible, and Transparent Graphene Films by Chemical Vapor Deposition for Organic Photovoltaics. *ACS Nano* **2010**, *4*, 2865−2873.

(5) Torrisi, F.; Hasan, T.; Wu, W.; Sun, Z.; Lombardo, A.; Kulmala, T. S.; Hsieh, G.-W.; Jung, S.; Bonaccorso, F.; Paul, P. J.; Chu, D.; Ferrari, A. C. Inkjet-Printed Graphene Electronics. *ACS Nano* **2012**, *6*, 2992−3006.

(6) Park, H.; Chang, S.; Zhou, X.; Kong, J.; Palacios, T.; Gradečak, S. Flexible Graphene Electrode-Based Organic Photovoltaics with Record-High Efficiency. *Nano Lett.* **2014**, *14*, 5148−5154.

(7) Bonaccorso, F.; Sun, Z.; Hasan, T.; Ferrari, A. C. Graphene Photonics and Optoelectronics. *Nat. Photonics* **2010**, *4*, 611−622.

(8) Meyer, J. C.; Geim, A. K.; Katsnelson, M. I.; Novoselov, K. S.; Booth, T. J.; Roth, S. The Structure of Suspended Graphene Sheets. *Nature* **2007**, *446*, 60−63.

(9) Zhu, W.; Low, T.; Perebeinos, V.; Bol, A. A.; Zhu, Y.; Yan, H.; Tersoff, J.; Avouris, P. Structure and Electronic Transport in Graphene Wrinkles. *Nano Lett.* **2012**, *12*, 3431−3436.

(10) Magda, G. Z.; Jin, X.; Hagymasi, I.; Vancso, P.; Osvath, Z.; Nemes-Incze, P.; Hwang, C.; Biro, L. P.; Tapaszto, L. Room-temperature Magnetic Order on Zigzag Edges of Narrow Graphene Nanoribbons. *Nature* **2014**, *514*, 608−611.

(11) Banhart, F.; Kotakoski, J.; Krasheninnikov, A. V. Structural Defects in Graphene. *ACS Nano* **2011**, *5*, 26−41.

(12) Pirkle, A.; Chan, J.; Venugopal, A.; Hinojos, D.; Magnuson, C. W.; McDonnell, S.; Colombo, L.; Vogel, E. M.; Ruoff, R. S.; Wallace, R. M. The Effect of Chemical Residues on the Physical and Electrical Properties of Chemical Vapor Deposited Graphene Transferred to SiO_2. *Appl. Phys. Lett.* **2011**, *99*, 122108.

(13) Khan, M. F.; Iqbal, M. Z.; Iqbal, M. W.; Eom, J. Improving the Electrical Properties of Graphene Layers by Chemical Doping. *Sci. Technol. Adv. Mater.* **2014**, *15*, 055004.

(14) Lu, C.-P.; Li, G.; Watanabe, K.; Taniguchi, T.; Andrei, E. Y. Choice Substrate for Accessing and Tuning the Electronic Properties of Graphene. *Phys. Rev. Lett.* **2014**, *113*, 156804.

(15) Wang, Z.; Tang, C.; Sachs, R.; Barlas, Y.; Shi, J. Proximity-Induced Ferromagnetism in Graphene Revealed by the Anomalous Hall Effect. *Phys. Rev. Lett.* **2015**, *114*, 016603.

DOI: 10.1021/acs.jpclett.5b02145
J. Phys. Chem. Lett. 2015, 6, 4437−4443

(16) Wang, Q. H.; Jin, Z.; Kim, K. K.; Hilmer, A. J.; Paulus, G. L. C.; Shih, C.-J.; Ham, M.-H.; Sanchez-Yamagishi, J. D.; Watanabe, K.; Taniguchi, T.; et al. Understanding and Controlling the Substrate Effect on Graphene Electron-Transfer Chemistry via Reactivity Imprint Lithography. *Nat. Chem.* **2012**, *4*, 724−732.
(17) Terrones, H.; Lv, R.; Terrones, M.; Dresselhaus, M. S. The Role of Defects and Doping in 2D Graphene Sheets and 1D Nanoribbons. *Rep. Prog. Phys.* **2012**, *75*, 062501.
(18) Lau, C. N.; Bao, W.; Velasco, J., Jr Properties of Suspended Graphene Membranes. *Mater. Today* **2012**, *15*, 238−245.
(19) Du, X.; Skachko, I.; Barker, A.; Andrei, E. Y. Approaching Ballistic Transport in Suspended Graphene. *Nat. Nanotechnol.* **2008**, *3*, 491−495.
(20) Bolotin, K. I.; Sikes, K. J.; Jiang, Z.; Klima, M.; Fudenberg, G.; Hone, J.; Kim, P.; Stormer, H. L. Ultrahigh Electron Mobility in Suspended Graphene. *Solid State Commun.* **2008**, *146*, 351−355.
(21) Maurand, R.; Rickhaus, P.; Makk, P.; Hess, S.; Tóvári, E.; Handschin, C.; Weiss, M.; Schönenberger, C. Fabrication of Ballistic Suspended Graphene with Local-Gating. *Carbon* **2014**, *79*, 486−492.
(22) Bernal, J. D. The Structure of Graphite. *Proc. R. Soc. London, Ser. A* **1924**, *106*, 749−773.
(23) Fitzer, E.; Kochling, K. H.; Boehm, H. P.; Marsh, H. Recommended Terminology for the Description of Carbon as a Solid. *Pure Appl. Chem.* **1995**, *67*, 473−506.
(24) Shibuta, Y.; Elliott, J. A. Interaction BetweenTtwo Graphene Sheets With a Turbostratic Orientational Relationship. *Chem. Phys. Lett.* **2011**, *512*, 146−150.
(25) Malard, L. M.; Pimenta, M. A.; Dresselhaus, G.; Dresselhaus, M. S. Raman Spectroscopy in Graphene. *Phys. Rep.* **2009**, *473*, 51−87.
(26) Cançado, L. G.; Jorio, A.; Pimenta, M. A. Measuring the Absolute Raman Cross Section of Nanographites as a Function of Laser Energy and Crystallite Size. *Phys. Rev. B: Condens. Matter Mater. Phys.* **2007**, *76*, 64304.
(27) Pimenta, M. A.; Dresselhaus, G.; Dresselhaus, M. S.; Cancado, L. G.; Jorio, A.; Saito, R. Studying Disorder in Graphite Based Systems by Raman Spectroscopy. *Phys. Chem. Chem. Phys.* **2007**, *9*, 1276−1290.
(28) Latil, S.; Meunier, V.; Henrard, L. Massless Fermions in Multilayer Graphitic Systems With Misoriented Layers: Ab Initio Calculations and Experimental Fingerprints. *Phys. Rev. B: Condens. Matter Mater. Phys.* **2007**, *76*, 201402.
(29) Kim, K.; Coh, S.; Tan, L. Z.; Regan, W.; Yuk, J. M.; Chatterjee, E.; Crommie, M. F.; Cohen, M. L.; Louie, S. G.; Zettl, A. Raman Spectroscopy Study of Rotated Double-Layer Graphene: Misorientation-Angle Dependence of Electronic Structure. *Phys. Rev. Lett.* **2012**, *108*, 246103.
(30) Hass, J.; de Heer, W. A.; Conrad, E. H. The Growth and Morphology of Epitaxial Multilayer Graphene. *J. Phys.: Condens. Matter* **2008**, *20*, 323202.
(31) Hass, J.; Varchon, F.; Millán-Otoya, J. E.; Sprinkle, M.; Sharma, N.; de Heer, W. A.; Berger, C.; First, P. N.; Magaud, L.; Conrad, E. H. Why Multilayer Graphene on 4H-SiC(0001) Behaves Like a Single Sheet of Graphene. *Phys. Rev. Lett.* **2008**, *100*, 125504.
(32) Ni, Z. H.; Chen, W.; Fan, X. F.; Kuo, J. L.; Yu, T.; Wee, A. T. S.; Shen, Z. X. Raman Spectroscopy of Epitaxial Graphene on a SiC Substrate. *Phys. Rev. B: Condens. Matter Mater. Phys.* **2008**, *77*, 115416.
(33) Mendes-de-Sa, T. G.; Goncalves, A. M. B.; Matos, M. J. S.; Coelho, P. M.; Magalhaes-Paniago, R.; Lacerda, R. G. Correlation Between (In)commensurate Domains of Multilayer Epitaxial Graphene Grown on SiC and Single Layer Electronic Behavior. *Nanotechnology* **2012**, *23*, 475602.
(34) Orlita, M.; Faugeras, C.; Plochocka, P.; Neugebauer, P.; Martinez, G.; Maude, D. K.; Barra, A. L.; Sprinkle, M.; Berger, C.; de Heer, W. A.; et al. Approaching the Dirac Point in High-Mobility Multilayer Epitaxial Graphene. *Phys. Rev. Lett.* **2008**, *101*, 267601.
(35) Lee, D. S.; Riedl, C.; Krauss, B.; von Klitzing, K.; Starke, U.; Smet, J. H. Raman Spectra of Epitaxial Graphene on SiC and of Epitaxial Graphene Transferred to SiO_2. *Nano Lett.* **2008**, *8*, 4320−4325.
(36) Mogera, U.; Kurra, N.; Radhakrishnan, D.; Narayana, C.; Kulkarni, G. U. Low Cost, Rapid Synthesis of Graphene on Ni: An Efficient Barrier for Corrosion and Thermal oxidation. *Carbon* **2014**, *78*, 384−391.
(37) Hauquier, F.; Alamarguy, D.; Viel, P.; Noël, S.; Filoramo, A.; Huc, V.; Houzé, F.; Palacin, S. Conductive-probe AFM Characterization of Graphene Sheets Bonded to Gold Surfaces. *Appl. Surf. Sci.* **2012**, *258*, 2920−2926.
(38) Kurra, N.; Prakash, G.; Basavaraja, S.; Fisher, T. S.; Kulkarni, G. U.; Reifenberger, R. G. Charge Storage in Mesoscopic Graphitic Islands Fabricated using AFM Bias Lithography. *Nanotechnology* **2011**, *22*, 245302.
(39) Vicarelli, L.; Heerema, S. J.; Dekker, C.; Zandbergen, H. W. Controlling Defects in Graphene for Optimizing the Electrical Properties of Graphene Nanodevices. *ACS Nano* **2015**, *9*, 3428−3435.
(40) Qi, Z. J.; Daniels, C.; Hong, S. J.; Park, Y. W.; Meunier, V.; Drndić, M.; Johnson, A. T. C. Electronic Transport of Recrystallized Freestanding Graphene Nanoribbons. *ACS Nano* **2015**, *9*, 3510−3520.
(41) Ferrari, A. C.; Basko, D. M. Raman Spectroscopy as a Versatile Tool for Studying the Properties of Graphene. *Nat. Nanotechnol.* **2013**, *8*, 235−246.
(42) Zhang, Y.; Zhang, L.; Zhou, C. Review of Chemical Vapor Deposition of Graphene and Related Applications. *Acc. Chem. Res.* **2013**, *46*, 2329−2339.
(43) Berciaud, S.; Ryu, S.; Brus, L. E.; Heinz, T. F. Probing the Intrinsic Properties of Exfoliated Graphene: Raman Spectroscopy of Free-Standing Monolayers. *Nano Lett.* **2009**, *9*, 346−352.
(44) Ni, Z. H.; Yu, T.; Luo, Z. Q.; Wang, Y. Y.; Liu, L.; Wong, C. P.; Miao, J.; Huang, W.; Shen, Z. X. Probing Charged Impurities in Suspended Graphene Using Raman Spectroscopy. *ACS Nano* **2009**, *3*, 569−574.
(45) Ni, Z.; Wang, Y.; Yu, T.; Shen, Z. Raman Spectroscopy and Imaging of Graphene. *Nano Res.* **2008**, *1*, 273−291.
(46) Ferrari, A. C.; Meyer, J. C.; Scardaci, V.; Casiraghi, C.; Lazzeri, M.; Mauri, F.; Piscanec, S.; Jiang, D.; Novoselov, K. S.; Roth, S.; et al. Raman Spectrum of Graphene and Graphene Layers. *Phys. Rev. Lett.* **2006**, *97*, 187401.
(47) Wang, G.; Zhang, M.; Zhu, Y.; Ding, G.; Jiang, D.; Guo, Q.; Liu, S.; Xie, X.; Chu, P. K.; Di, Z.; et al. Direct Growth of Graphene Film on Germanium Substrate. *Sci. Rep.* **2013**, *3*, 2465.
(48) Wilson, N. R.; Pandey, P. A.; Beanland, R.; Young, R. J.; Kinloch, I. A.; Gong, L.; Liu, Z.; Suenaga, K.; Rourke, J. P.; York.; et al. Graphene Oxide: Structural Analysis and Application as a Highly Transparent Support for Electron Microscopy. *ACS Nano* **2009**, *3*, 2547−2556.
(49) Wu, Q.; Jung, S. J.; Jang, S. K.; Lee, J.; Jeon, I.; Suh, H.; Kim, Y. H.; Lee, Y. H.; Lee, S.; Song, Y. J. Controllable Poly-crystalline Bilayered and Multilayered Graphene Film Growth by Reciprocal Chemical Vapor Deposition. *Nanoscale* **2015**, *7*, 10357−10361.
(50) He, B.; Ren, Z.; Yan, S.; Wang, Z. Large Area Uniformly Oriented Multilayer Graphene With High Transparency and Conducting Properties Derived From Highly Oriented Polyethylene Films. *J. Mater. Chem. C* **2014**, *2*, 6048−6055.
(51) Cançado, L. G.; Takai, K.; Enoki, T.; Endo, M.; Kim, Y. A.; Mizusaki, H.; Speziali, N. L.; Jorio, A.; Pimenta, M. A. Measuring the Degree of Stacking Order in Graphite by Raman Spectroscopy. *Carbon* **2008**, *46*, 272−275.
(52) Kumar, G. V. P.; Narayana, C. Adapting a Fluorescence Microscope to Perfrom Surface Enhanced Raman Spectroscopy. *Curr. Sci.* **2007**, *93*, 778−781.

DOI: 10.1021/acs.jpclett.5b02145
J. Phys. Chem. Lett. 2015, 6, 4437−4443